JOM
https://doi.org/10.1007/s11837-024-06819-5

TECHNICAL ARTICLE

(Hf,Zr,W,Mo,Ti)B_2 High-Entropy Boride Ceramics Fabricated by Boro/Carbothermal Reduction Method Combined with SPS

BOYU NI,[1] YAN ZHANG,[1,2,4] HUI ZOU,[1] SHUANGYU LIU,[1] LEI SHAN,[1,5] HAIYAN SHI,[3] ZHAOYU LV,[3] and ZEHAO HE[3]

1.—School of Mechanical and Electrical Engineering, Shaoxing Key Laboratory of Mechanical Components Surface and Interface Science, Shaoxing University, Shaoxing 312000, China. 2.—School of Mechanical and Electrical Engineering, Tianjin University, Tianjin 300072, China. 3.—Zhejiang Fengqiu Kerui Pump Industry Limited Company, Zhuji 311800, China. 4.—e-mail: 935308551@qq.com. 5.—e-mail: shanlei@usx.edu.cn

In order to further improve the density and properties of high-entropy boride ceramics, (Hf,Zr,W,Mo,Ti)B_2 high-entropy boride ceramics were prepared by boro/carbothermal reduction combined with SPS. The phase composition, microstructure, and mechanical properties of the ceramics were studied, and the results showed that (Hf,Zr,W,Mo,Ti)B_2 high-entropy boride powder contained a highentropy phase, an oxides impurities phase, a WB phase, and a HfB_2 phase at 1600 °C. After sintering at 2000 °C, there was no oxide impurity in the (Hf,Zr,W,Mo,Ti)B_2 high-entropy boride ceramics, which consisted of a high-entropy phase and a small amount of WB second phase. The hardness and fracture toughness were 29.9 ± 1.0 GPa and 3.36 ± 0.21 MPa·$m^{1/2}$, respectively. The hardness was higher than the high-entropy boride ceramics with the same components prepared by in situ reactive sintering and borothermal reduction. The mechanical properties of the high-entropy ceramics obtained by boro/carbothermal reduction was excellent. and were higher than those reported in the literature of the same component.

INTRODUCTION

In recent years, high-entropy ceramics has shown a better performance than traditional ceramic materials because of their special "high-entropy effect". For example, high-entropy borides (HEBs) are characterized by a high melting point, good thermal stability, and high chemical stability, showing good mechanical and anti-oxidant capacity.[1] In addition, HEBs can also realize the oriented design of performance through the flexible design of their components, so that they can adapt to different application environment requirements.[2–4] Gild et al. used high-energy ball milling combined with spark plasma sintering (SPS) at 2000 °C to prepare a series of high-entropy pressure boride ceramics $(Hf_{0.2}Zr_{0.2}Ta_{0.2}Nb_{0.2}Ti_{0.2})B_2$, $(Hf_{0.2}Zr_{0.2}Ta_{0.2}Mo_{0.2}Ti_{0.2})B_2$, $(Hf_{0.2}Zr_{0.2}Mo_{0.2}Nb_{0.2}Ti_{0.2})B_2$,$(Hf_{0.2}Mo_{0.2}Ta_{0.2}Nb_{0.2}Ti_{0.2})B_2$,$(Mo_{0.2}Zr_{0.2}Ta_{0.2}Nb_{0.2}Ti_{0.2})B_2$, ($(Hf_{0.2}Zr_{0.2}W_{0.2}Mo_{0.2}Ti_{0.2})B_2$, and $((Hf_{0.2}Zr_{0.2}Ta_{0.2}Cr_{0.2}Ti_{0.2})B_2$) for the first time.[5] They found that, compared with binary boride ceramics, high-entropy boride ceramics had higher hardness and better oxidation resistance, but their density was only 92%. Zhang et al. used borothermal reduction to improve the density of high-entropy boride ceramics by increasing the purity of the powder, so as to further improve the mechanical properties of the materials. The average particle size of the prepared $(Hf_{0.2}Zr_{0.2}W_{0.2}Mo_{0.2}Ti_{0.2})B_2$ powder was 0.44 μm, and the relative density was > 94%.[6] The hardness reached 27.7 GPa, higher than other high-entropy diboride ceramics reported in the literature (relative density was about 92%, hardness was about 17.5 ~ 23.7 GPa).[5] Gild et al. found that boro/carbothermal reduction could significantly improve the purity of high-entropy boride powder, and a dense (> 99%) $(Hf_{0.2}Zr_{0.2}Ta_{0.2}Nb_{0.2}Ti_{0.2})B_2$ high-entropy boride ceramic was fabricated.[7] Zhang et al. studied the preparation of HEB-SiC composites by

(Received June 3, 2024; accepted July 26, 2024)

Published online: 20 August 2024

boro/carbothermal reduction and borothermal reduction, and the results showed that, compared with HEB-SiC prepared by borothermal reduction, ceramics prepared by boro/carbothermal reduction have finer microstructure and higher Vickers hardness value.[8]

In addition, high-entropy boride ceramic mechanical properties could also be improved through dissolving different metal elements, as Qin et al. reported.[9] The study found that the hardness of $(Zr_{0.2}Nb_{0.2}Ta_{0.2}Ti_{0.2}Mo_{0.2})B_2$ containing Mo elements was 24.9 ± 1.3 GPa, and it reached 26.7 ± 1.1 GPa for $(Hf_{0.2}Zr_{0.2}Ta_{0.2}W_{0.2}Mo_{0.2})B_2$, both containing Mo and W elements. However, the hardness of $(Hf_{0.2}Zr_{0.2}Nb_{0.2}Ta_{0.2}Ti_{0.2})B_2$ with no W and Mo elements was only 16.4 GPa. The comparison showed that Mo and W had significant effects on improving the hardness of high-entropy boride ceramics. On the one hand, it might be caused by the" "cocktail" effect of high entropy,[10] while, on the other hand, the introduction of transition elements, leading to more *p–d* hybridization,[11] which would increase the hardness of high-entropy boride ceramics by enhancing bonding, reducing lattice distortion, increasing electron density, changing the band structure, and forming a short-range ordered structure.[12–14]

In summary, in order to refine the particle size of the powder promoting the densification of high-entropy boride ceramics and to improve the mechanical properties, in this article, $(Hf,Zr,W,Mo,Ti)B_2$ high-entropy boride ceramics was fabricated by boro/carbothermal reduction combined with SPS, and the phase composition, microstructure, and mechanical properties have been investigated.

EXPERIMENTAL METHODOLOGY

Sample Preparation

In this experiment, HfO_2 (average particle size: 0.3 μm, purity 99.95%; Beijing Pantech Technology), ZrO_2 (average particle size: 0.6 μm, purity 99.8%; Changsha Xili Nano Grinding Technology), TiO_2 (average particle size: 21 nm, purity 99.9%; Xuancheng Jingshui New Materials), MoO_3 (average particle size: 1 μm, purity 99.9%; Shanghai Nai 'ou Nano Technology), and WO_3 (average particle size: $\sim$ 1.0 μm, purity 99.9%; Shanghai Xiangtian Nanomaterials), powders were used as oxide raw materials. According to the target product of $(Hf_{0.2}Zr_{0.2}W_{0.2}Mo_{0.2}Ti_{0.2})B_2$, the transition metal oxide powder was combined with B_4C (average particle size: $\sim$ 1.5 μm, purity $\geq$ 99.9%; Mudanjiang Diamond Boron Carbide) and graphite powder (average particle size: $\sim$ 2.0 μm, purity $\geq$ 99.9%; Shanghai Colloidal Chemical Factory) for weighing. In order to compensate for the loss of boron sources during the boro/carbothermic reduction reaction, B_4C powder was oversupplied by 20 wt.% and the content of C powder was reduced accordingly. The weighed powder was placed in a polyethylene tank containing Si_3N_4 medium and ethanol by ball milling for 24 h, after which the ball-milled powder was dried by rotary evaporation. After grinding through a 100-mesh sieve to obtain a dry powder mixture, the mixed powder was pressed into small pieces by a tablet press and put into a graphite crucible (diameter 30 mm, thickness 5 mm), followed by vacuum heat treatment for 1 h at 1600 °C at a heating rate of 10 °C/min in a unpressured sintering furnace (LHS-2; Zhongshan Kaishen Vacuum Technology Engineering). The $(Hf,Zr,W,Mo,Ti)B_2$ target product powder was obtained. The synthesized high-entropy ceramic powder was ground by a 100-mesh sieve and then loaded into a graphite moldwhich was put into a spark plasma sintering furnace (H-HPD10-FL; FCTSysteme) to obtain the $(Hf,Zr,W,Mo,Ti)B_2$ ceramic. The SPS sintering furnace had a sintering temperature of 2000 °C holding for 10 min in an Ar atmosphere, the heating rate was 150 °C/min, and the pressure was 30 MPa.

Experimental Test Methods

Thermodynamics calculation was conducted on HSC Chemistry 6.0 software.[15] X-ray diffraction (XRD; Cu-Kα; D8, Bruker, Germany) analyzed the phase composition of the high-entropy boride powder and ceramic at a scanning rate of 10°/min and a scanning range of 20–90°. The X-ray spectra were refined by using GSAS software, and quantitative phase analysis results were obtained.[16] Scanning electron microscopy (SEM; NovaNanoSEM430; FEI, USA) and energy dispersive spectroscopy (EDS; X-MarN; Oxford) were used to study the microstructure of the high-entropy boride powder, and the composition and fracture morphology of the ceramic. The sample for EDS was polished using 1000- and 2000-mesh abrasive paper to grind in turn after planishing with 400- and 800-mesh diamond polishing discs. The specific surface area of the powder was determined by a nitrogen adsorption analyzer (SA3100; Beckman Coulter). Assuming that it was spherical, its average particle size (d) was calculated from the specific surface area.[17] The grain size of the high-entropy boride ceramics was measured using Nano Measure software, which was calculated according to the average value of at least 100 grains after acid etching on the polished surface (the $HF:HNO_3:H_2O$ volume ratio = 1:1:3). The density of the sintered body was measured by the Archimedean drainage method and the theoretical density of the sintered body was obtained by the mixing law. A HVS-30Z microhardness tester (GB/T16534-2009) was used to test the Vickers hardness at no less than 10 points for each sample within 15 s under a load of 1.96 N.[18] The room-temperature fracture toughness was measured by indentation on the Vickers hardness tester (HVS–30Z/LCD; Temin Optical Instrument, Shanghai, China).[19] At least 10

points were selected for each sample, and the load was 98 N holding for 10 s.

RESULTS AND DISCUSSION

Thermodynamic Analysis

The possible reaction equations for the synthesis of (Hf,Zr,W,Mo,Ti)B_2 powder by boro/carbothermal reduction reaction were:

$$HfO_2(s) + 1/2B_4C + 3/2C(s) = HfB_2(s) + 2CO(g) \quad (1)$$

$$ZrO_2(s) + 1/2B_4C + 3/2C(s) = ZrB_2(s) + 2CO(g) \quad (2)$$

$$WO_3(s) + 1/2B_4C + 5/2C(s) = WB_2(s) + 3CO(g) \quad (3)$$

$$MoO_3(s) + 1/2B_4C + 5/2C(s) = MoB_2(s) + 3CO(g) \quad (4)$$

$$TiO_2(s) + 1/2B_4C + 3/2C(s) = TiB_2(s) + 2CO(g) \quad (5)$$

$$HfO_2(s) + ZrO_2(s) + WO_3(s) + MoO_3(s) + TiO_2(s) + 0.5B_4C + 11.5C(s) = (Hf, Zr, W, Mo, Ti)B_2 + 12CO(g) \quad (6)$$

With the database module of HSC Chemistry 6.0 software, thermodynamic analysis of Eqs. 1–5 could be performed. According to previous studies, the boro/carbothermal reduction method requires a two-step reaction to achieve. For the first step, the transition metal oxides of five elements first reacted with B_4C to generate the corresponding borides and B_2O_3.[20] Then the B_2O_3 proceeded to react with the oxides and carbon sources of the five elements to form further borides. B_2O_3 had a low vapor pressure and volatilized below 1450 °C; therefore, in order to compensate for the loss of boron source caused by volatilization of B_2O_3, an excess of 20 wt.% B_4C was added, and the content of C was accordingly reduced.

Figure 1 shows the change trend of Gibbs free energy of five oxides (HfO_2, MoO_3, WO_3, TiO_2, and ZrO_2) reacting with B_4C and C calculated by the thermodynamic calculation module, as a function of temperature.

It can be seen from the figure that, when the Gibbs free energy ΔG was less than 0, the boro/carbothermal reduction reaction began to occur, and the above reaction equation could be carried out. As can be seen from Fig. 1, the boro/carbothermal reduction reaction of MoO_3 had the fastest reaction speed at the beginning, followed by WO_3, and HfO_2 was the last reaction. The first and last reaction temperatures were 392.64 °C and 1451.56 °C, respectively. HfO_2 began to react when the temperature exceeded 1451.56 °C, and all the reactions could react spontaneously, so, in this experiment, it was needed to determine only the synthesis temperature of HfB_2. The reaction temperature for the synthesis of HfB_2 powder by boro/carbothermal reaction was generally required to be greater than 1550°C.[21–24] In order to ensure that the boro/carbothermal reaction was carried out more thoroughly and the solution reaction was complete, the synthesis of (Hf,Zr,W,Mo,Ti)B_2 high-entropy boride powder was determined at 1600 °C.

Phase Composition Analysis

Figure 2 shows the XRD patterns of high-entropy boride powders and ceramics. As can be seen from Fig. 2a, the high-entropy (Hf,Zr,W,Mo,Ti)B_2, WB, and HfB_2 phases were detected after the boro/carbothermal reduction reaction at 1600 °C/1 h. Compared with the standard diffraction peak of HfB_2 (PDF38-1398), the diffraction peak of the high-entropy phase was similar to the diffraction peak of HfB_2, but was shifted to a higher 2θ. Because the ionic sizes of Zr, W, Mo, and Ti were smaller than Hf, the dissolution of Zr, W, Mo, and Ti into the lattice of HfB_2 caused a decrease of the lattice parameters. In addition, a small amount of (Hf,Zr)O_2 oxide impurities were also detected in the powder, and the boro/carbothermal reduction reaction of ZrO_2 and HfO_2 occurred later than the other oxides (as shown in Fig. 1), so there were unreacted oxide phases and undissolved HfB_2 phases at 1600 °C. As shown in Fig. 2b, after sintering at 2000°C, the high-entropy boride phase was the dominant phase. Compared with the standard diffraction peak of HfB_2 (PDF38-1398) and high-entropy boride powder (Fig. 2a), it was shifted to a higher 2θ, and the lattice

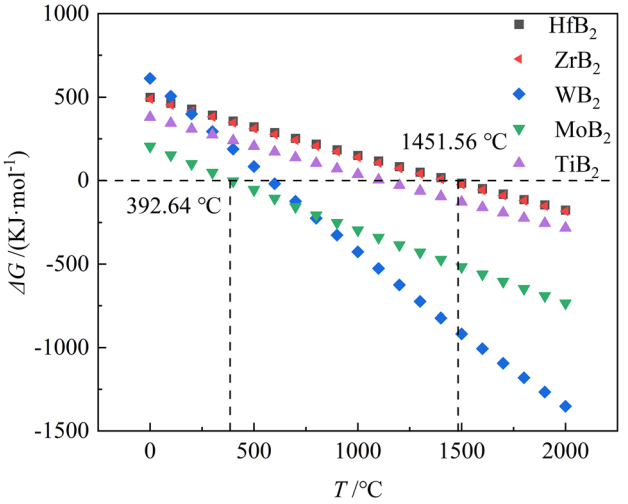

Fig. 1. Curves of ΔG with T in five boron/carbothermal reactions of oxides

constant of the high-entropy ceramic became smaller. The HfB_2 phase and oxide impurity phase were not detected in the high-entropy ceramic, indicating that the boro/carbothermal reaction and the solid dissolution of the HfB_2 phase into the high-entropy phase matrix were further promoted by the increasing temperature.

Because WB had an orthogonal structure, which was different from the lattice structure of the high-entropy phase (hexagonal structure), the solid-solution rate and the solid solubility were lower than the other borides.[25] As a result, there was still undissolved WB phase in the $(Hf,Zr,W,Mo,Ti)B_2$ high-entropy boride ceramic.

Figure 3 shows the Rietveld fitting and finishing results of high-entropy boride ceramics. The fitting and finishing results were R_{wp} = 22.68% and R_p = 15.19%, respectively. The Rietveld fitting result showed that the content of the high-entropy phase of $(Hf,Zr,W,Mo,Ti)B_2$ was 97.23 wt.%, and the second phase of WB was 2.77 wt.%. The lattice constants of the $(Hf,Zr,W,Mo,Ti)B_2$ high entropy phase are obtained by GSAS finishing software as $a = b =$ 3.0917 Å and c = 3.3792 Å lower than that of HfB_2 ($a = b$ = 3.1438 Å, c = 3.4793 Å).[26,27] Since the atomic sizes of Zr, W, Mo, and Ti were smaller than those of the Hf element, when they dissolved into the HfB_2 lattice, this resulted in the decrease of the lattice constants.[5] WB may increase the residual stress, but the specific amount needs to be studied in the later stage. The existence of WB makes the five elements of the high-entropy phase deviate from the equimolar ratio. For the high-entropy ceramics, the lattice constants of the high-entropy phase will increase, and the diffraction peak position shifts to the low angle, but, because WB (orthogonal structure) was inconsistent with the crystal form of the HfB_2/high entropy phase (hexagonal structure), the diffusion activation energy was higher for the formation of a solid solution. Therefore, the WB diffusion rate slows down, and there was still undissolved WB phase in the sample, affecting the high-entropy phase X-ray peak positions.[6]

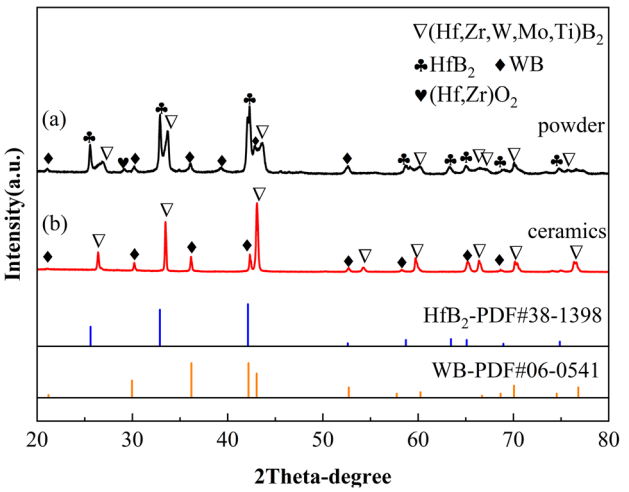

Fig. 2. XRD patterns of high-entropy boride powders and ceramics

Microscopic Composition Analysis

Figure 4 shows the SEM image of high-entropy boride powder $(Hf,Zr,W,Mo,Ti)B_2$, from which it can be seen that the powder had agglomeration. The specific surface area of the $(Hf,Zr,W,Mo,Ti)B_2$ sample was 1.83 m^2/g, the equivalent average particle size was 0.39 ± 0.21 μm, and the average particle size of $(Hf_{0.2}Zr_{0.2}W_{0.2}Mo_{0.2}Ti_{0.2})B_2$ high-entropy powder prepared by borothermal reduction was 0.44 μm. Because B_2O_3 was an intermediate

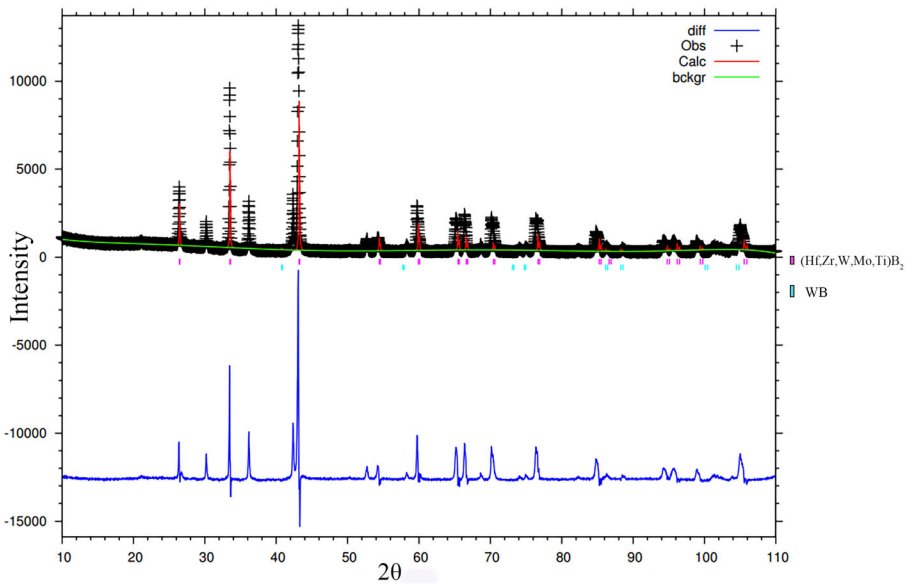

Fig. 3. Rietveld fitting of XRD data for high-entropy boride ceramics

product in the boro/carbothermal reduction, it could react quickly and the evaporation and condensation was weakened, inhibiting the coarsening of the powder particle size. Therefore, compared with the borothermal reduction method (0.44 μm),[6] the particle size of the high-entropy boride powder synthesized by the boro/carbothermal reduction method was finer (0.39 $\pm$ 0.21 μm).

Figure 5a shows the fracture morphology of the (Hf,Zr,W,Mo,Ti)B_2 high-entropy boride ceramics, the fracture form of (Hf,Zr,W,Mo,Ti)B_2 was transgranular fracture, and it can be seen that there were some pores. However, due to the existence of the secondary phase of the WB phase and the complex composition, the theoretical density of (Hf,Zr,W,Mo,Ti)B_2 was difficult to calculate. Therefore, the relative density of the (Hf,Zr,W,Mo,Ti)B_2 sample is not reported in this work. From image analysis, the relative density appears to be greater than 98% (i.e., with less than 2 vol.% of pores). Figure 5b shows the etching morphology of the polished surface of the (Hf,Zr,W,Mo,Ti)B_2 high-entropy boride ceramics with the grain size of 1.01 $\pm$ 0.2 μm, which was smaller than that of the high-entropy ceramics with the same elements prepared by borothermal reduction (3.12 μm) and in situ reactive sintering (14.7 $\pm$ 12.4 μm).[28] In addition, a large number of white particles can be observed in Fig. 5b, which are located at the grain boundary and triple junction of the (Hf,Zr,W,Mo,-Ti)B_2 matrix. Combined with the previous XRD analysis, this was the WB second phase, and the average particle size was 0.72 μm.

Figure 6 shows the EDS map scanning element distribution images of the (Hf,Zr,W,Mo,Ti)B_2 high-entropy boride ceramics, from which it can be seen that the surface contains a gray phase and a white phase. Five elements, of Hf, Zr, W, Mo, and Ti, were detected in the gray phase, and the five elements were evenly distributed. It was proved that the gray phase was a high-entropy phase. In the white phase, an obvious aggregation phenomenon of the W element can be seen, as similarly reported in Refs. 5, 6, and 29. Combined with the XRD analysis, this confirms that this was the WB second phase.

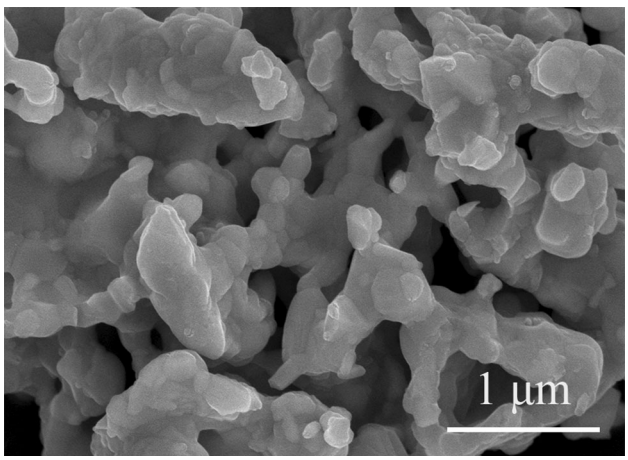

Fig. 4. SEM image of high-entropy boride powder

Mechanical Property

In addition, (Hf,Zr,W,Mo,Ti)B_2 had a better performance than HfB_2, ZrB_2, WB_2, MoB_2, or TiB_2. This was because the atomic sizes of Zr, W, Mo. and Ti elements are smaller than Hf, which induced lattice distortion in the high-entropy ceramics during the process of dissolving into the Hf lattice to form the high-entropy phase. As a result, it hindered the movement of dislocation, and increased the hardness of the material.[37] The fracture toughness of (Hf,Zr,W,Mo,Ti)B_2 was 3.36 $\pm$ 0.21 MPa·$m^{1/2}$, which was similar to those reported in the literature.[20]

CONCLUSION

HfO_2, ZrO_2, WO_3, MoO_3, TiO_2, B_4C, and graphite were used as raw materials to synthesize (Hf,Zr,W,Mo,Ti)B_2 high-entropy boride powder by boro/carbothermal reduction, and high-entropy boride ceramics were prepared by SPS at 2000 °C. The

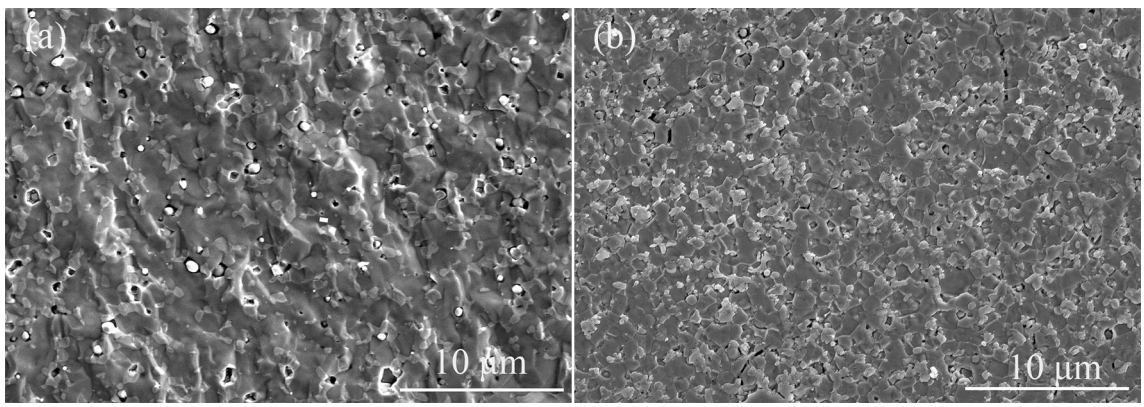

Fig. 5. High-entropy boride ceramics: (a) fracture morphology, (b) etching morphology of polished surfaces

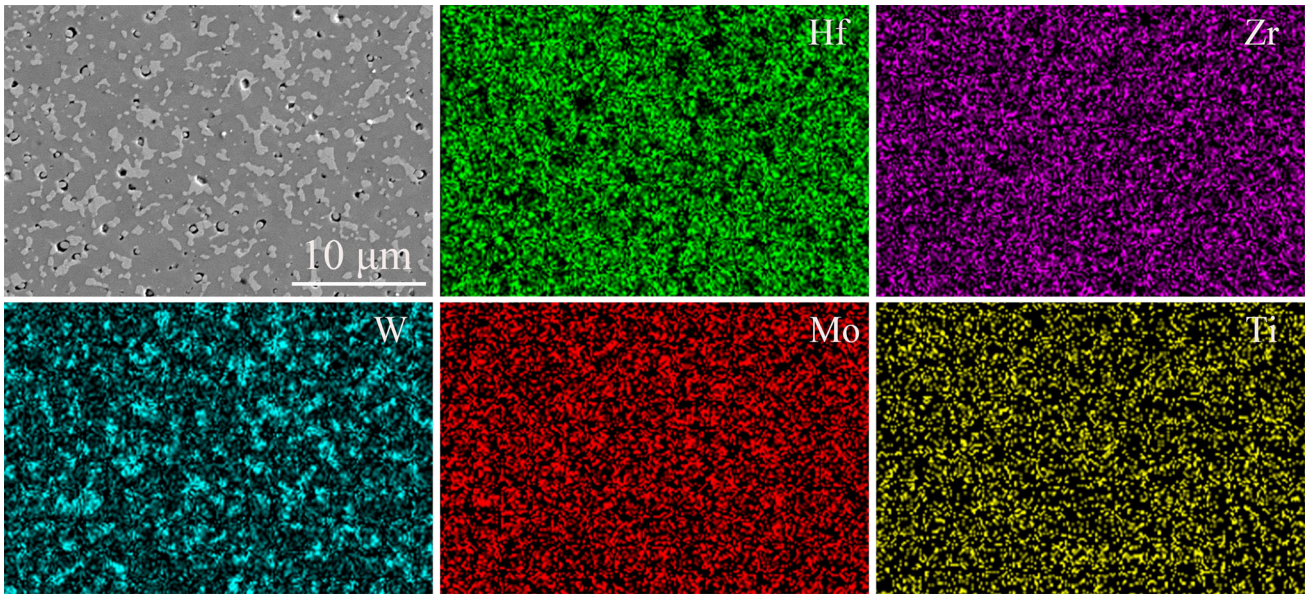

Fig. 6. Mapping element distribution of high-entropy boride ceramics polished surface

Table 1. (Hf,Zr,W,Mo,Ti)B_2 comparison of mechanical properties of ceramics with the literature[6,24,28,31–36]

Composition	Density (%)	$H_{v0.2}$ (GPa)	Fracture toughness/(MPa·$m^{1/2}$)
(Hf,Zr,W,Mo,Ti)B_2	–	29.9 ± 1.0	3.36 ± 0.21
$(Hf_{0.2}Zr_{0.2}W_{0.2}Mo_{0.2}Ti_{0.2})B_2$[6]	–	27	–
$(Hf_{0.2}Zr_{0.2}W_{0.2}Mo_{0.2}Ti_{0.2})B_2$[28]	97.5	26.0 ± 1.5	–
$(Hf_{0.2}Zr_{0.2}Ta_{0.2}Mo_{0.2}Ti_{0.2})B_2$[32]	96	23.4 ± 1.2	3.67 ± 0.62
$(Hf_{0.2}Zr_{0.2}Ta_{0.2}V_{0.2}Ti_{0.2})B_2$[31]	93.1	22.9 ± 1.2	3.32 ± 0.44
HfB_2[24]	98.8	18.1 ± 0.9	3.5 ± 0.5
ZrB_2[33]	99.8	23 ± 0.9	3.5 ± 0.3
WB_2[34]	97.86	24.4 ± 0.4	–
MoB_2[35]	–	21.3–24.2	–
TiB_2[36]	96.1	28.6–32.4	4.64 ± 0.45

phase composition, microstructure, and mechanical properties of (Hf,Zr,W,Mo,Ti)B_2 powder and ceramics were studied. The results show that:

(1) (Hf,Zr,W,Mo,Ti)B_2 powder was dominated by the high-entropy phase, and there were a HfB_2 phase, a WB phase, and a small amount of (Hf,Zr)O_2 phase at 1600 °C. After sintering at 2000 °C, (Hf,Zr,W,Mo,Ti)B_2 high-entropy ceramics were composed of a high-entropy phase and a WB second phase.

(2) (Hf,Zr,W,Mo,Ti)B_2 high-entropy boride ceramics prepared by boro/carbothermal reduction combined with SPS had excellent mechanical properties, and the hardness and fracture toughness were 29.9 ± 1.0 GPa and 3.36 ± 0.21 MPa·$m^{1/2}$, respectively. The hardness was higher than that of high-entropy boride ceramics without the W and Mo elements, and also higher than the high-entropy boride ceramics with the same components prepared by in situ reactive sintering and borothermal reduction.

ACKNOWLEDGEMENTS

This work was financially supported by the Basic public welfare program projects in Shaoxing city (No. 2023A11005), Zhuji "Reveal the list and take charge" project (No. 2022J24)

CONFLICT OF INTEREST

On behalf of all authors, the corresponding author states that there is no conflict of interest.

REFERENCES

1. L. Backman, J. Gild, J. Luo, and J. Elizabeth, *Acta Mater.* 197, 20 https://doi.org/10.1016/j.actamat.2020.07.003 (2020).
2. L. Feng, W.G. Fahrenholtz, and D.W. Brenner, *Annu. Rev. Mater. Res.* 51(1), 165 https://doi.org/10.1146/annurev-matsci-080819-121217 (2021).

3. B. Storr, L. Moore, and K. Chakrabarty, *APL Mater.* 10(6), 061109 (2022).
4. P.B. Zhao, J.B. Zhu, K.J. Yang, M. Li, G. Shao, H. Lu, Z. Ma, H. Wang, and J. He, *Appl. Surf. Sci.* 616, 156516 https://doi.org/10.1016/j.apsusc.2023.156516 (2023).
5. J. Gild, Y.Y. Zhang, T. Harrington, S. Jiang, T. Hu, M.C. Quinn, W.M. Mellor, N.X. Zhou, K. Vecchio, and J. Luo, *Sci. Rep.* 6(1), 37946 https://doi.org/10.1038/srep37946 (2016).
6. Y. Zhang, S.K. Sun, W. Zhang, Y. You, W.M. Guo, Z.W. Chen, J.H. Yuan, and H.T. Lin, *Ceramics Int.* https://doi.org/10.1016/j.ceramint.2020.02.214 (2020).
7. J. Gild, A. Wright, Q.T. Kathleen, M. Qin, and J. Luo, *Ceramic Int.* 46(5), 6906 https://doi.org/10.1016/j.ceramint.2019.11.186 (2019).
8. Y. Zhang, S.K. Sun, W.M. Guo, L. Xu, and H.T. Lin, *J. Adv. Ceram* 10(1), 173 (2020).
9. M. Qin, J. Gild, H. Wang, T. Harrington, K.S. Vecchio, and J. Luo, *J. Eur. Ceram. Soc.* 40(12), 4348 (2019).
10. F.Z. Dai, Y.C. Zhou, and W. Sun, *Acta Mater.* 127, 312 https://doi.org/10.1016/j.actamat.2017.01.048 (2017).
11. H. Wang, S. Lee, and H. Kim, *J. Am. Ceram. Soc.* 95, 1493 https://doi.org/10.1111/j.1551-2916.2012.05141.x (2012).
12. E.P. George, W.A. Curtin, and C.C. Tasan, *Acta Mater.* 188, 435 https://doi.org/10.1016/j.actamat.2019.12.015 (2020).
13. H. Ren, R.R. Chen, X.F. Gao, T. Liu, G. Qin, Y.L. Chiu, S.P. Wu, and J.J. Guo, *Rare Metals.* 43(01), 324 https://doi.org/10.1007/S12598-023-02410-0 (2024).
14. P. Ansh, K. Modalavalasa, and A.K. Prasada Rao, *Sci. Rep.* 14(1), 7692 https://doi.org/10.1038/S41598-024-57094-Y (2024).
15. B. Cheynet. *Thermodynamic properties of inorganic materials: a literature database covering the period* 1970-1987.(Canada, Elsevier Science Pub.Co., 1989), pp.1-20.
16. B.H. Toby, Expgui. *J. Appl. Crystallogr.* 34, 210 (2001).
17. K. Hendrik, G. Beaucage, R. Mueller, and E. Sotiris, *PubMed.* 20(5), 1915 https://doi.org/10.1021/la030155v (2004).
18. Standardization Administration of China. *China Zhijian Publishing House.* GB/T16534−2009 (2009).
19. A.G. Evans and E.A. Charles, *J. Am. Ceram.* 59, 371 https://doi.org/10.1111/j.1151-2916.1976.tb10991.x (1976).
20. X.Q. Shen, J.X. Liu, F. Li, and G.J. Zhang, *Ceramics Int.* 45(18), 24508 https://doi.org/10.1016/j.ceramint.2019.08.178 (2019).
21. W.M. Guo, L.X. Wu, S.K. Sun, and H. Lin, *J. Am. Ceram.* 100(2), 524 https://doi.org/10.1111/jace.14693 (2017).
22. W.M. Guo, D.W. Tan, L.Y. Zeng, L.L. Hao, T.W. Hua, and Y. Cheng, *Ceram. Int.* 44, 4473 (2018).
23. W.M. Guo and G.J. Zhang, *J. Am. Ceram.* 92(1), 264 https://doi.org/10.1111/j.1551-2916.2008.02836.x (2009).
24. D.W. Ni, G.J. Zhang, Y.M. Kan, and P.L. Wang, *Int. J. Appl. Ceram Tech.* 7(6), 830 https://doi.org/10.1111/j.1744-7402.2009.02404.x (2010).
25. O.Y. Ishizawa, *J. Alloys Compd.* 221(1/2), 8 https://doi.org/10.1016/0925-8388(94)01486-8 (1995).
26. L. Bsenko and T. Lundstrom, *JLCM.* 34, 273 https://doi.org/10.1016/0022-5088(74)90169-6 (1974).
27. S.S. Shukla, *Int. Mater.* 20(1), 5045 https://doi.org/10.1179/174328005X14267 (2005).
28. M.D. Qin, J. Gild, H.R. Wang, T. Harrington, K.S. Vecchio, and J. Luo, *J. Eur. Ceram. Soc. Ceram Soc.* 40(12), 4348 https://doi.org/10.1016/j.jeurceramsoc.2020.03.063 (2020).
29. B.Y. Ni, Y. Zhang, and L. Shan, *JOM.* https://doi.org/10.1007/s11837-024-06715-y (2024).
30. C.C. Wang, L.L. Song, and Y.P. Xie, *Materials.* 13(5), 1212 https://doi.org/10.3390/ma13051212 (2020).
31. Z.J. Huang, Y. Zhang, W.M. Guo, L. Xu, and W. Zhang, *AMCS* 39(5), 2405 (2022).
32. X.T. Li, Z.F. Wei, Y.F. Zu, G.Q. Chen, X.S. Fu, and W.L. Zhou, *J. Ceram. Sci. Technol.* 44(04), 688 (2023).
33. A.L. Chamberlain, W.G. Fahrenholtz, G.E. Hilmas, and D.T. Ellerby, *J. Am. Ceram.* 87(6), 1170 https://doi.org/10.1111/j.1551-2916.2004.01170.x (2023).
34. B. Liu, *Guangdong University of Technology.* (2023).
35. B. Olofinjana, G.O. Egharevba, M.A. Eleruja, C. Jeynes, A.V. Adedeji, O.O. Akinwunmi, B.A. Taleatu, C.U. Mordi, and E.O.B. Ajayi, *JMST.* 26(6), 552 https://doi.org/10.1016/S1005-0302(10)60084-9 (2010).
36. A. Mukhopadhyay, G.B. Raju, B. Basu, and A.K. Suri, *J Eur Ceram Soc.* 29(3), 505 https://doi.org/10.1016/j.jeurceramsoc.2008.06.030 (2009).
37. Y. Zhang, L. Shan, Y.F. Chai, W.M. Guo, T.Q. Zhang, L. Xu, J.L. Cong, H.T. Lin, L.Y. Wei, and W.M. Ma, *Ceram. Int.* 49(10), 16029 https://doi.org/10.1016/J.CERAMINT.2023.01.200 (2024).